Tuning the Mobility Coupling of Quaternized Polyvinylpyridine and Anionic Phospholipids in Supported Lipid Bilayers

ARTICLE *in* LANGMUIR · JANUARY 2015

Impact Factor: 4.46 · DOI: 10.1021/la504241w · Source: PubMed

5 AUTHORS, INCLUDING:

Xiaojun Shi

University of Akron

8 PUBLICATIONS **7** CITATIONS

SEE PROFILE

Xiaodong Zhuang

Technische Universität Dresden

58 PUBLICATIONS **928** CITATIONS

SEE PROFILE

Adam Smith

University of Akron

34 PUBLICATIONS **804** CITATIONS

SEE PROFILE

Langmuir

Article

pubs.acs.org/Langmuir

Tuning the Mobility Coupling of Quaternized Polyvinylpyridine and Anionic Phospholipids in Supported Lipid Bilayers

Xiaojun Shi,[†] Xiaosi Li,[†] Megan J. Kaliszewski,[†] Xiaodong Zhuang,[‡] and Adam W. Smith*[,†]

[†]Department of Chemistry, The University of Akron, 190 Buchtel Common, Akron, Ohio 44325-3601, United States

[‡]Institute of Advanced Organic Materials, School of Chemistry and Chemical Engineering, Shanghai Jiao Tong University, 315 Jiangong Building, 800 Dongchuan Road, Shanghai 200240, China

Supporting Information

ABSTRACT: Binding of biomacromolecules to anionic lipids in the plasma membrane is a common motif in many cell signaling pathways. Previous work has shown that macromolecules with cationic sequences can form nanodomains with sequestered anionic lipids, which alters the lateral distribution and mobility of the membrane lipids. Such sequestration is believed to result from the formation of a lipid−macromolecule complex. To date, however, the molecular structure and dynamics of the lipid−polymer interface are poorly understood. We have investigated the behavior of polycationic quaternized polyvinylpyridine (QPVP) on supported lipid bilayers doped with phosphatidylserine (PS) or phosphatidylinositol phosphate (PIP) lipids using time-resolved fluorescence microscopy, including pulsed interleaved excitation fluorescence cross-correlation spectroscopy (PIE-FCCS). PIE-FCCS is a dual-color fluorescence spectroscopy that translates fluctuations in fluorescence signal into a measurement of diffusion and colocalization. By labeling the polymer and lipids, we investigated the adsorption-induced translational mobility of lipids and systematically studied the influence of lipid charge density and solution ionic strength. Our results show that alteration of anionic lipid lateral mobility is dependent on the net charge of the lipid headgroup and is modulated by the ionic strength of the solution, indicating that electrostatic interactions drive the decrease in lateral mobility of anionic lipids by adsorbed QPVP. At physiological salt concentration we observe that the lipid lateral mobility is weakly influenced by QPVP and that there is no evidence of stable lipid−polymer complexes.

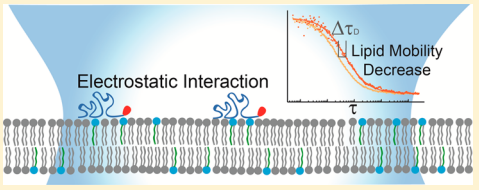

INTRODUCTION

Interactions between peripheral membrane proteins and lipids in the plasma membrane are crucial to many cell signaling events. Numerous peripheral membrane proteins contain polybasic regions that are thought to interact with the negatively charged inner leaflet of the plasma membrane.[1−3] Binding of these cationic macromolecules with the plasma membrane is believed to alter the lateral distribution and translational mobility of anionic lipids.[4,5] Early electron spin resonance studies provided spectroscopic evidence of bulk interactions between anionic lipids and cationic biomacromolecules.[6] To date, however, the dynamics of the lipid−macromolecule interface, the strength of the interactions, and the role of electrostatics remain unresolved. In this report we address these questions in model supported lipid bilayers using time-resolved fluorescence spectroscopy. We find that a polycationic macromolecule, quaternized polyvinylpyridine (QPVP), does hinder the mobility of anionic lipids, but that the effect is significantly modulated by lipid charge and buffer ionic strength.

Anionic phospholipids are abundant in the inner leaflet of the plasma membrane.[3] Phosphatidylserine (PS) and phosphatidylglycerol (PG), which carry a single negative charge on the headgroup, comprise ∼10% of all lipids in the plasma membrane.[7] Phosphatidylinositol phosphate (PIP) lipids can have one to three phosphates on the inositol ring, which allows a PIP lipid to carry two to four negative charges at physiological pH.[8,9] These low abundance anionic phospholipids (∼1% of the total lipids in the inner leaflet of the plasma membrane[2]) have important physiological functions, including activation of ion channels, modulation of peripheral proteins, and cytoskeletal attachment.[3,8,10] Anionic lipids interact with peripheral cationic macromolecules such as peptides with polybasic amino acid sequences or proteins that have positively charged surfaces or binding pockets. Previous work has shown that these lipid−macromolecule interactions can cause changes in the lateral distribution and mobility of the anionic lipids.[3,4,11]

Simulations show that cationic macromolecules can segregate phosphatidylinositol biphosphate (PIP_2) lipids causing heterogeneity in the PIP_2 distribution,[12−14] while PS molecules only enrich around the macromolecule.[5,12] Despite previous experimental efforts to investigate the interaction between oppositely charged lipid membranes and macromolecules,[2,5,6,15−17] the structure and dynamics of these interactions are still not well-understood. McLaughlin et al. reported that the mobility of tail-labeled PIP_2 on the inner leaflet of the plasma membrane is lower than it is on the outer leaflet, and they proposed that the reduced diffusion of PIP_2 on the inner

Received: October 28, 2014
Revised: January 15, 2015
Published: January 19, 2015

DOI: 10.1021/la504241w
Langmuir 2015, 31, 1784−1791

leaflet is due to electrostatic interactions with membrane proteins containing unstructured clusters of basic residues.[11] In model membranes, a similar mobility reduction was observed by measuring the diffusion coefficient of headgroup-labeled phosphoethanolamine (PE) lipids (net charge of −1) in a supported lipid bilayer carrying ionic polyelectrolytes.[18] Two modes of lipid diffusion with different mobilities were found. Lipids with fast diffusion were assigned to free lipids, while lipids with a reduced diffusion coefficient were interpreted to be transiently trapped within polymer nanodomains. The authors described this phenomenon as slaved lipid diffusion, meaning that the lipid mobility is governed by interactions with multivalent polymer nanodomains. The lipid mobility reduction was not affected by the different charges of the polyelectrolytes, which suggests that the interactions may not have been driven by electrostatics and could have been influenced by interactions with the lipid headgroup fluorophore.

Despite its importance in cell signaling and physiology, a systematic investigation of the diffusion of anionic lipids in response to different levels of electrostatic interaction with cationic polyelectrolytes has not yet been reported experimentally. Although it has been proposed by many simulation[12,14,19−21] and experimental studies,[2,5,6,16] direct evidence of collective diffusion resulting from lipid segregation around macromolecules is still not available. In this paper, a labeled cationic polyelectrolyte, QPVP, was adsorbed onto supported lipid bilayers containing tail-labeled lipids with anionic headgroups. The diffusion of the labeled lipids and labeled QPVP was investigated with pulsed interleaved excitation fluorescence cross-correlation spectroscopy (PIE-FCCS) which quantifies the concentration and mobility of the lipids and polymers simultaneously and measures the degree of correlated diffusion. PIE-FCCS has been used in the past to resolve membrane protein−protein interactions and oligomerization,[22,23] but has not been applied to directly probe lipid−protein cross-correlation. In previous simulation studies, several facts were considered to have significant impact on the strength of the electrostatic interaction between polyelectrolytes and lipids, including charge density on the lipid headgroup, charge density of the adsorbing polyelectrolytes (charge of segment, polymer chain length, polymer configuration, etc.), and the ionic strength of the supporting buffer.[12,13] Here we show that the translational mobility of the anionic lipids was reduced by the adsorbed polyelectrolyte, but that the effect was strongly dependent on lipid headgroup charge and the ionic strength of the supporting buffer. For PS lipids at physiological salt concentrations no mobility reduction was observed upon addition of the polyelectrolyte. While the coupling between PIP_2 lipids and polyelectrolyte is strong enough to alter the translational mobility of lipids, no direct evidence of collective diffusion of lipids and polymers or the existence of polymer−lipid complexes was found.

MATERIALS AND METHODS

Reagents. 1,2-Dioleoyl-*sn*-glycero-3-phosphatidylcholine (DOPC), 1-palmitoyl-2-(dipyrromethene boron difluoride)undecanoyl-*sn*-glycero-3-phospho-L-serine (Top Fluor-PS), 1,2-dioleoyl-*sn*-glycero-3-phospho-L-serine (DOPS), and 1-oleoyl-2-[6-[4-(dipyrromethene boron difluoride)butanoyl]amino]hexanoyl-*sn*-glycero-3-phosphoinositol-4,5-bisphosphate (Top Fluor-PI(4,5)P_2) were purchased from Avanti Polar Lipids (Alabaster, AL). The molecular structures of Top Fluor-PS and Top Fluor-PI(4,5)P_2 are shown in Scheme 1. Alexa Fluor 568 hydrazide was purchased from Life Technologies (Carlsbad, CA). QPVP was synthesized in house using RAFT polymerization (see

Scheme 1. Molecular Structures of Alexa Fluor 568-Labeled QPVP, Top Fluor-PS, and Top Fluor-PI(4,5)P_2

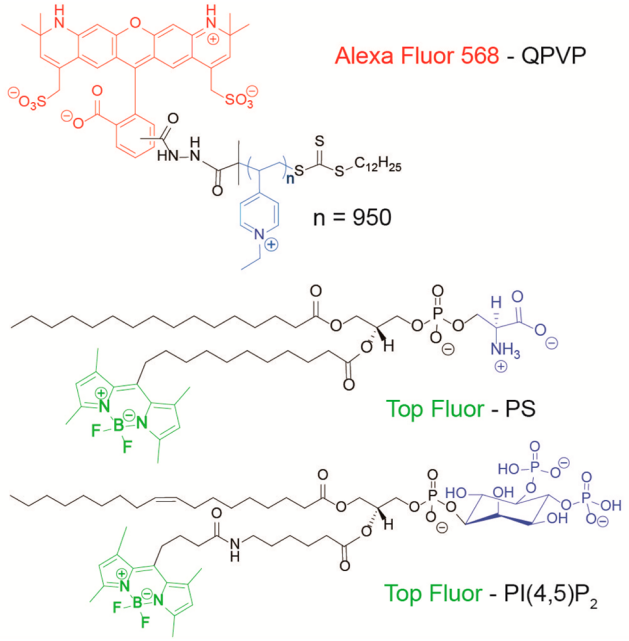

below for details). Three different concentrations of PBS solution (pH 7.3) were prepared for use as working buffers: buffer **P1**, 1 mM sodium phosphate, 10 mM sodium chloride, 100 nM EDTA; buffer **P5**, 5 mM sodium phosphate, 50 mM sodium chloride, 100 nM EDTA; buffer **P10**, 10 mM sodium phosphate, 100 mM sodium chloride, 100 nM EDTA. All water used here is Milli-Q water.

Custom synthesized nucleic strands consisted of a noncomplementary sequence of 41 nucleotides [CCC TAG AGT GAG TCG TAT GAT AGT GAC AGC TGG ATC GTT AC] with fluorescence tags of 6-carboxyfluorescein (FAM) and/or carboxy-tetramethylrhodamine (TAMRA) (Integrated DNA Technologies). FAM has a maximum excitation and emission at 495 and 520 nm, respectively. TAMRA has excitation and emission wavelengths of 559 and 583 nm. A dual-labeled oligonucleotide, referred to as dl-ssDNA in this work, contains TAMRA at the 5′ end and FAM at the 3′ end of the sequence above. A 100 nM solution of dl-ssDNA is used as an FCCS positive control. A mixture of two single-labeled oligonucleotides (one with TAMRA at the 5′ end and the other with FAM at the 3′ end of the sequence above) was used as a negative control (50 nM of each). We refer to this sample as sl-ssDNA. Both control samples were measured in 10 mM TRIS buffer at pH = 7.8.

Preparation of Alexa Fluor 568 Labeled Quaternized Polyvinylpyridine (QPVP). *S*-1-Dodecyl-*S*′-(*a*,*a*′-dimethyl-*a*′-acetic acid) trithiocarbonate (DDAT) was synthesized according to the reported method.[24] Reversible addition−fragmentation chain transfer (RAFT) polymerization is used to prepare polyvinylpyridine (PVP). The polymerization of 4-vinylpyridine with the RAFT agent, DDAT, was conducted with the following procedure. A mixture of DDAT (9.6 mg, 0.026 mmol), 4-vinylpyridine (VP; 1.0 g, 9.5 mmol), azobis-(isobutyronitrile) (AIBN; 1.4 mg, 0.0086 mmol), and DMF (1.5 mL) was degassed by three freeze−pump−thaw cycles and then stirred at 70 °C under nitrogen atmosphere for 24 h. After terminating the reaction, the mixture was redispersed in DMF, stirred, precipitated into 50 mL of ethyl ether, and filtered. Such procedures were used to remove the residual monomer and initiator. After filtration and wash with ethyl ether, the precipitation was dried overnight under reduced pressure to give PVP. The molecular weight was determined by GPC in DMF to be 100 161 g/mol. PVP (1 mg) was redissolved in chloroform and stirred with excess bromoethane overnight. The precipitate was collected as quaternized PVP (QPVP). Carboxy-terminated QPVP was dissolved in DI water and reacted with Alexa Fluor 568 hydrazide through EDC coupling overnight. Labeled QPVP

DOI: 10.1021/la504241w
Langmuir 2015, 31, 1784−1791

was dialyzed against Milli-Q water for 2 days to remove the residual dyes. The molecular structure of Alexa Fluor 568 QPVP is shown in Scheme 1.

Preparation of Phospholipid Vesicles. DOPC and TopFluor-PS (TF-PS, 0.005 mol %) lipids were dissolved in chloroform, and DOPC and TopFluor-PI(4,5)P_2 (TF-PIP_2, 0.01 mol %) lipids were dissolved in chloroform/methanol/water (9.0:0.8:0.2), dried under vacuum, and resuspended in water, yielding a concentration of 1 mg/mL lipid vesicle suspension. The lipid vesicle suspension was extruded through a porous membrane (100 nm diameter) 15 times to yield a small unilamellar vesicle (SUV) suspension.

Preparation of Supported Lipid Bilayers (SLBs). Glass coverslips were sonicated in IPA/water (50:50) solution for 30 min, followed by an additional 30 min sonication in pure water to remove dust and contaminants. After cleaning, the coverslips were soaked in piranha solution (a fresh-made 3:1 mixture of sulfuric acid and 30% hydrogen peroxide) for 10 min, rinsed extensively with water, and then dried under a stream of nitrogen gas. A 30 μL volume of the SUV suspension was mixed with 30 μL of 1X PBS and deposited on a coverslip in an AttoFluor sample chamber (Life Technologies, Carlsbad, CA) and incubated 5 min at room temperature. After bilayer formation, the sample was washed and rinsed with 30 mL of water and carefully exchanged to the desired buffer. The fluidity of SLBs was checked using FRAP before PIE-FCCS measurements. After preparation of the SLB, the buffer in the sample chamber was exchanged with 5 nM labeled QPVP in the working buffer. Samples were incubated at room temperature and observed within 90 min of preparation.

PIE-FCCS Instrumentation. Fluorescence measurements were made on an inverted microscope with custom-built modules for fluorescence excitation and detection (Figure 1). The excitation source is a supercontinuum white light fiber laser (SuperK NKT Photonics, Birkerod, Denmark). The pulse rate is set to 9.7 MHz with a pulse duration of 5 ps. A wavelength splitter picks off a 488 nm (±10 nm) beam while the 561 nm light is separated by a 561 nm (±20 nm) dichroic (z405/561rpc, Chroma Technology Corp, Bellows Falls, VT). The rest of the white light is directed to a beam dump. The beams pass through a respective narrow-band cleanup filter (488: LL01-488-12.5, Semrock, Rochester, NY; 561: LL02-561-12.5, Semrock, Rochester, NY) before being coupled into a single-mode optical fiber (488: QPMJ-3AF3U-488-3.5/125-3AS-18-1-SP, OZ Optics, Ottawa, Ontario; 561:QPMJ-3AF3U-488-3.5/125-3AS-3-1-SP, OZ Optics, Ottawa, Ontario). In order to delay the second pulse from the prompt pulse by a delay of at least 50 ns, the fibers differ in length by about 15 m. After traveling through separate optical fibers, each beam is collimated with identical infinity corrected objective lenses (L-10x, Newport, Irvine, CA) and is independently set for select laser power by continuously variable ND filters (Thorlabs Inc., Newton, NJ). The two beams are spatially overlapped using a 503 nm cutoff dichroic beamsplitter (LM01-503-25, Semrock, Rochester, NY) and directed into the optical path of the microscope using a TIRF filter block (zt488/561rpc and zet488/561m, Chroma Technology Corp., Bellows Falls, VT). A 100X TIRF objective, NA 1.49 (Nikon Corp., Tokyo, Japan), is used for imaging and PIE-FCCS measurements.

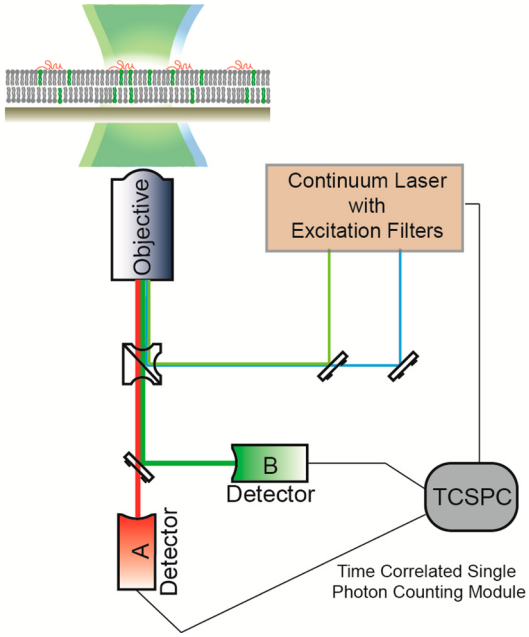

Figure 1. Schematic of dual-color pulsed interleaved excitation–fluorescence cross-correlation spectroscopy. Excitation laser beams (488 and 561 nm) are directed from a continuum laser source by using excitation filters and are sent to the objective through a dichroic mirror. Excitation beams are focused in the samples, in which the fluorophores will be excited. The fluorescence emission is collected through the objective and separated from the excitation light by the dichroic mirror. A pinhole (not shown) is used before the beam splitter; the emission light passing through is detected by two APDs. The leaving time of the excitation laser pulses and the arriving time of emission laser pulses are synchronized by a TCSPC module.

The fluorescence signal enters the detection module through a 50 micron pinhole (Thorlabs, Newton, NJ) for confocal detection and is collimated with a 100 mm focal length achromatic lens (AC254-100-A-ML, Thorlabs Inc., Newton, NJ). A 560 nm long-pass filter (FF560-FDi01-25 × 36, Semrock, Rochester, NY) is used to split the light into two spectral channels. Two band-pass filters (green, 520/44 nm [FF01-520/44-25]; red, 612/69 nm [FF01-621/69-25]) are used to isolate the spectral range of each detection channels. The spectrally filtered beam is focused onto a single photon avalanche diode (SPAD) detector (Micro Photon Devices, Bolzano, Italy) by a 50 mm focal length lens (APAC18, Newport Corp. Irvine, CA). The signal is collected by a time-correlated single photon counting module (Picoharp 300, PicoQuant, Berlin, Germany) synchronized with the white light fiber laser source.

PIE-FCCS Data Analysis. In fluorescence correlation spectroscopy (FCS), temporal fluctuations in the fluorescence signal are autocorrelated with respect to a lag time, τ. The normalized autocorrelation function (ACF) is defined by

$$G(\tau) = \frac{\langle \delta F(t+\tau)\delta F(t)\rangle}{\langle F(t)\rangle^2}$$

where $\langle\rangle$ stands for time average and $F(t)$ is fluorescence intensity at time t. The plot of the ACF versus lag time produces a curve that describes the mobility and concentration of the ensemble during the acquisition time within the Rayleigh-limited confocal volume. Dual color excitation is used in FCCS to quantify interactions between two differently labeled species. The cross-correlation of the two detection channels reveals the population of codiffusing species. From the relative populations of all the species present in a sample, the degree of oligomerization can be determined.

In cross-correlation spectroscopy, fluorescence fluctuations in each detection channel are cross-correlated (CCF). In our experiment, the two channels are labeled red and green and the CCF becomes

$$G_{r\times g}(\tau) = \frac{\langle \delta F_r(t+\tau)\cdot\delta F_g(t)\rangle}{\langle F_r(t)\rangle\langle F_g(t)\rangle}$$

In the event of equal molecular brightness (and lack of significant energy transfer or quenching), the amplitude of the correlation function is directly related to the relative population, N, of each species of diffusing fluorophore. The amplitude in each channel is then

$$G_r(0) = \frac{1}{\langle N_r + N_{rg}\rangle}$$

$$G_g(0) = \frac{1}{\langle N_g + N_{rg}\rangle}$$

DOI: 10.1021/la504241w
Langmuir 2015, 31, 1784–1791

$$G_{r\times g}(0) = \frac{N_{rg}}{\langle N_g + N_{rg}\rangle\langle N_r + N_{rg}\rangle} = G_r(0)*G_g(0)*N_{rg}$$

The correlation curve in the confocal volume is related to the Brownian dynamics through the dwell time, τ_D

$$G(\tau) = G(0)\frac{1}{\left(1 + \frac{\tau}{\tau_D}\right)}$$

in which

$$\tau_D = \frac{\omega_0^2}{4D}$$

where ω_0 is the lateral distance where the excitation intensity reaches $1/e^2$ of its value from the center of the confocal volume and D is the diffusion coefficient of the fluorescent molecule (typically reported in $\mu m^2/s$). On our instrument the detection radius, ω_0, of 488 and 561 nm focal beams is 0.21 and 0.23 μm, respectively.

The degree of oligomerization, f_c, is determined by a ratio of the relative populations

$$f_c = \frac{N_{rg}}{\min[(N_r + N_{rg}), (N_g + N_{rg})]}$$

Values for f_c range from 0 to 1, indicating zero codiffusion to complete codiffusion.

A model for anomalous diffusion is used to fit the experimental ACF and CCF curves. The theoretical correlation function includes an anomalous correction factor (α):

$$G(\tau) = \frac{1}{\langle N\rangle}\frac{1}{\left(1 + \frac{\tau}{\tau_D}\right)^{\alpha}}$$

When α is 1, the diffusion is Brownian motion; if $0 < \alpha < 1$, the diffusion is anomalous motion. The triplet lifetime is much shorter than the dwell time of lipids and polymers; hence, this factor is not considered in the fitting and normalization of correlation function.

RESULTS

Cross-Correlation in FCCS Standards. FCCS is a powerful tool to quantify the degree of interaction between two populations of molecules.[25] Here we define the degree of binding by f_c as described in the Materials and Methods section. The two populations are labeled with two different color fluorophores which inevitably have some degree of spectral overlap. This spectral overlap causes false cross-correlation and hence an overestimation of the degree of binding. With pulsed interleaved excitation (PIE), the arrival times of the emission photons are recorded and used to discriminate photons arriving from spectral cross-talk.[26] With this temporal filter, PIE-FCCS renders a more accurate measurement of binding than FCCS without PIE. Figure 2 shows the ACF and CCF of sl-ssDNA (FCCS negative control, Figure 2, bottom) and dl-ssDNA (FCCS positive control, Figure 2, top) calculated with the temporal filter as PIE-FCCS (Figure 2, left column) or as traditional FCCS without PIE (Figure 2, right column). For the negative control (Figure 2, bottom), the CCF from PIE-FCCS measurement is essentially 0 ($f_c = 0.001$) while the f_c calculated from FCCS without PIE measurement is larger (0.06). This effect is much larger for fluorophores with broader emission spectra like fluorescent proteins.[23] Similarly, FCCS without PIE measurement gave a larger f_c value (0.854) than PIE-FCCS did ($f_c = 0.826$) for the positive control. The PIE-FCCS measurement of the positive control provided a fraction correlated less than 100% ($f_c = 0.826$ or 83%) which is assigned to two well-known artifacts. The first is that some

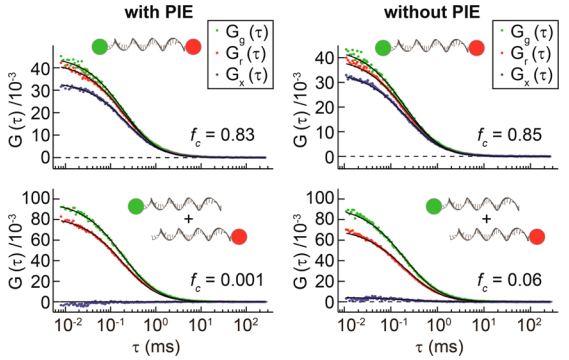

Figure 2. FCCS measurements of labeled DNA are analyzed with (left) and without (right) the PIE time-gate analysis. The FCS data in the top graphs correspond to the dl-ssDNA sample described in the Materials and Methods and represent a positive control for cross-correlation. The bottom graphs correspond to the sl-ssDNA sample and represent a negative control for cross-correlation.

population of the ssDNA is either missing a tag or else it has a fluorescent tag that is no longer fluorescent. The second artifact is the imperfect overlap of the two confocal volumes due to chromatic aberrations.[25] Our value for the fraction correlated is comparable to other previously published positive controls for FCCS.[25−27]

Synthesis and Labeling of QPVP. QPVP is a cationic polyelectrolyte that can interact with negatively charged membrane lipids. It has been used in redox batteries as anion exchange membrane,[28] and in water treatment to prevent corrosion.[29] It has been widely studied for application as an antibiotic,[30] and as a vehicle for gene delivery.[31] QPVP is synthesized via quaternization of polyvinylpyridine (PVP) which is polymerized from vinylpyridine monomers via reversible addition−fragmentation chain transfer (RAFT) polymerization.[32] The novelty of RAFT polymerization is that the polymerization degree can be easily controlled so that the product has a relatively narrow distribution of molecular weights. Gel permeation chromatography (GPC) results indicate the molecular weight of PVP used in this study is around 100 000 g/mol. Absorption spectra and FCS measurements of fluorescently-labeled QPVP are consistent with single-labeled QPVP and no detectable concentration of free dye in solution (Supporting Information Figure S1). According to the diffusion coefficient extracted from three-dimensional FCS measurement of labeled QPVP solution, the hydrodynamic radius (R_h) of QPVP chain is around 22 nm.

Adsorption of QPVP on DOPC SLBs Doped with TopFluor-PI(4,5)P_2 (TF-PIP_2). Supported lipid bilayers (SLBs) were prepared by rupture of small unilamellar vesicles (SUVs) on glass substrate. The lipid vesicles were composed of 99.99% DOPC and 0.01% TF-PIP_2. Epi-fluorescence imaging (Supporting Information Figure S2) indicates the SLBs are uniform and without major defects. It is known that the inositol ring of the PIP_2 molecule has a strong interaction with the supporting glass substrate.[33] Because of this interaction, the TF-PIP_2 lipids on the bottom leaflet interact strongly to the glass substrate. After photobleaching a defined area, FRAP experiments (Supporting Information Figure S2) indicate that 40% of the fluorescence intensity is recovered, corresponding to the recovery of mobile TF-PIP_2 lipids on the top leaflet. FCS measurements in the recovered area show that TF-PIP_2 lipids

DOI: 10.1021/la504241w
Langmuir 2015, 31, 1784−1791

on the top leaflet undergo free Brownian motion. (Figure 4 and Supporting Information Figure S4)

In the experiments described below, labeled QPVP is added to the buffer above the SLBs where it encounters the bilayer lipids. Any electrostatic interactions between the charged molecules can be modulated by adjusting the ionic strength of the supporting buffer. High ionic strength buffer results in strong electrostatic screening effects and will weaken electrostatic interactions between the charged molecules. In order to investigate the lipid diffusion with and without adsorbing QPVP at different solution screening levels, experiments were carried out in three different buffer conditions: 1 mM sodium phosphate, 10 mM sodium chloride, pH 7.3 (buffer **P1**); 5 mM sodium phosphate, 50 mM sodium chloride, pH 7.3 (buffer **P5**); and 10 mM sodium phosphate, 100 mM sodium chloride, pH 7.3 (buffer **P10**).

Upon adsorption of QPVP to the SLB, the epi-fluorescence image of QPVP shows two polymer populations. Figure 3A–C shows images of TF-PIP$_2$ bilayer carrying QPVP in buffer **P5**. A time average of QPVP images (Figure 3B) shows bright punctate clusters of fluorescence in a background of even intensity. The clusters are immobile over several minutes and are assigned to aggregated clusters of QPVP. Areas of lower intensity are populated by mobile QPVP as evidenced by FRAP and FCS. The polymer surface coverage between the immobile clusters is extracted from the FCS data and is approximately 0.01%. We obtain this estimate from the size of the confocal detection area (0.166 μm^2), the average number of polymers in the area (~1.5), and the area per polymer (0.0015 μm^2) calculated using the R_h (22 nm) from the FCS data (Supporting Information Figure S1). Recently, Arteta et al. reported that polycationic dendrimers also interact with anionic SLBs and that they can both translocate through SLBs and rest on top of SLBs.[34]

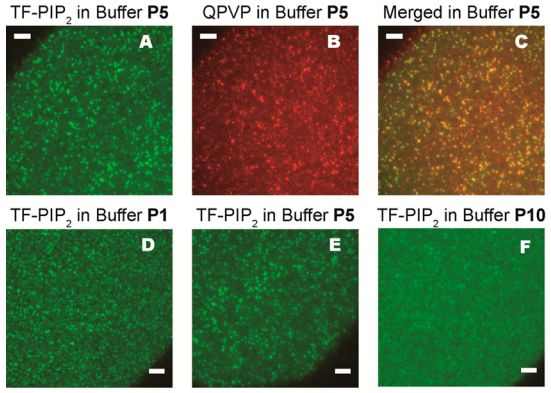

Figure 3. Epi-fluorescence images of bilayers with 0.01% TF-PIP$_2$ and adsorbed QPVP. In panels A–C the images of the lipid and polymer species are compared for buffer P5. Panel A shows the fluorescence image of TF-PIP$_2$. Panel B shows the fluorescence of QPVP by averaging 60 time-lapse images collected over several seconds. Panel C is the merged image of panels A and B, showing a high degree of overlap between the immobile lipid and polymer clusters. In panels D–F, the spatial distribution of TF-PIP$_2$ lipids is shown for the three solvent conditions: buffer P1 (D), buffer P5 (E), and buffer P10 (F). At the highest salt concentration, bright punctate lipid clusters around the QPVP clusters are no longer observed. All scale bars are 5 μm.

The fluorescence image corresponding to TF-PIP$_2$ (Figure 3A) shows a lipid distribution similar to that of the polymer in buffer **P5**: a population of bright, immobile clusters in a background of mobile lipid. By overlapping the images of lipid and QPVP, QPVP clusters and TF-PIP$_2$ clusters were found to be highly colocalized (Figure 3C), showing that TF-PIP$_2$ lipids were segregated by QPVP clusters at this buffer condition. FRAP measurements (Supporting Information Figure S3) showed that the fluorescence intensity of the TF-PIP$_2$ clusters can recover after photobleaching, indicating that the clusters are not amorphous lipid aggregates, but are fluid and coupled to the surrounding SLB. Because the lipids remain fluid in the cluster areas, we conclude that TF-PIP$_2$ can still diffuse from segregating QPVP cluster into the mobile fraction and those in the mobile fraction can diffuse back into segregating QPVP cluster. Due to the low mobility of the TF-PIP$_2$ lipids in the clusters, we were not able to obtain well-defined FCS curves to investigate the dynamics of TF-PIP$_2$ inside the cluster.

The TF-PIP$_2$ clusters were observed at low ionic strength buffer (buffer **P1**) (Figure 3D), where the electrostatic interaction between TF-PIP$_2$ and QPVP is the strongest. By increasing the ionic strength of the supporting buffer, the electrostatic interaction will be screened and hence weakened. In buffer **P5**, the TF-PIP$_2$ clusters are still observable (Figure 3E). However, in buffer **P10**, which has the strongest electrostatic screening effect, there are no punctate, immobile TF-PIP$_2$ clusters (Figure 3F), indicating that the immobile QPVP clusters no longer sequester TF-PIP$_2$ molecules. The dependence of TF-PIP$_2$ cluster formation on different buffer conditions indicates that the sequestration of TF-PIP$_2$ around QPVP clusters results from electrostatic interactions between the two populations.

PIE-FCCS Measurements of TF-PIP$_2$ in the SLBs with Adsorbed QPVP. The diffusion coefficient of TF-PIP$_2$ lipids in the SLB was extracted from FCS measurements in different buffers. Autocorrelation curves of TF-PIP$_2$ in the original bilayer and with bound QPVP in the mobile fraction of bilayer are shown in Figure 4, where the inflection point of the autocorrelation curve indicates the average dwell time of TF-PIP$_2$ lipids in the laser focus. For the supported bilayers without QPVP, no significant change was observed in the lipid mobility over the three buffer conditions studied here (Figure 4D). This is consistent with earlier work, where no variation in lipid

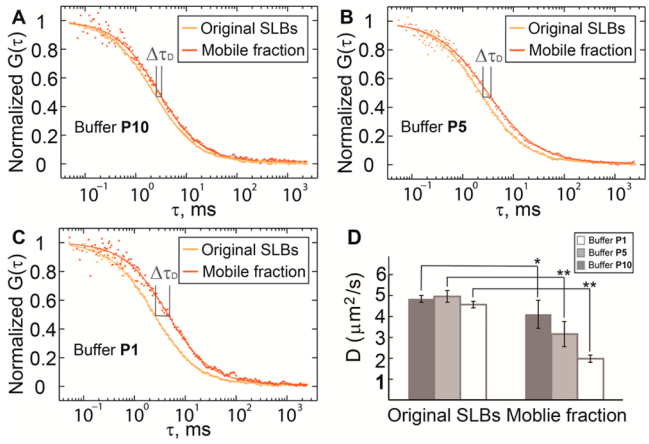

Figure 4. Autocorrelation curves of TF-PIP$_2$ in original SLBs (orange), at mobile fraction (red) of SLBs carrying QPVP in buffer **P1** (A), buffer **P5** (B), and buffer **P10** (C). (D) Diffusion coefficients for TF-PIP$_2$ in buffer **P1** (white column), buffer **P5** (light gray column), and buffer **P10** (dark gray column). The diffusion coefficients are the average of 10 measurements on two SLBs (* p = 0.006, ** p < 0.001).

DOI: 10.1021/la504241w
Langmuir 2015, 31, 1784–1791

mobility was observed over a similar range of electrolyte concentrations.[35] Upon adsorption of QPVP, the TF-PIP$_2$ lipid mobility decreases. The change of dwell time ($\Delta\tau_D$) of TF-PIP$_2$ due to QPVP adsorption indicates the effect of the mobile adsorbed polymer on the diffusion of the underlying lipids. The mobility of the TF-PIP$_2$ lipids in the presence of adsorbed QPVP varies from high ionic strength buffer to low ionic strength buffer (Figure 4A–C). The diffusion coefficients of TF-PIP$_2$ in the original bilayer and with adsorbed QPVP are, respectively, 4.84 ± 0.16 and 4.11 ± 0.67 $\mu m^2/s$ in buffer **P10**, 4.96 ± 0.28 and 3.16 ± 0.60 $\mu m^2/s$ in buffer **P5**, and 4.57 ± 0.15 and 1.98 ± 0.17 $\mu m^2/s$ in buffer **P1**. This means that the mobility of TF-PIP$_2$ decreased 15.2% in buffer **P10** after QPVP adsorption, and 36.3% and 56.6% in buffer **P5** and buffer **P1**, respectively. Combined, these data show that the diffusion of TF-PIP$_2$ is slaved to QPVP. The fact that this slaved diffusion can be screened with high ionic strength buffer indicates that TF-PIP$_2$ mobility is coupled to QPVP through electrostatic interactions.

One strength of PIE-FCCS is its ability to resolve the correlated diffusion of two labeled populations of molecules. If, for example, the adsorbed QPVP diffuses as a complex or nanodomain with a stable population of TF-PIP$_2$ lipids bound, we would expect to see nonzero amplitude in the early time value of the cross-correlation function. Our data show zero cross-correlation (i.e., f_c = 0) at all buffer conditions (Supporting Information Figure S5), indicating that there is no detectable population of long-lived (>6 ms) lipid–polymer complexes.

The FCS data for TF-PIP$_2$ lipids in supported lipid bilayers fit well to a standard 2D Brownian diffusion model. Upon adsorption of the polymer, however, the curves showed a small-amplitude, long-time component that fit well to an anomalous diffusion model (see Materials and Methods). In the model function, α is an exponent used to describe the degree of anomalous diffusion. When α is 1, the diffusion is Brownian; if $0 < \alpha < 1$, the diffusion is anomalous. The α value was 0.98 for TF-PIP$_2$ motion in original bilayers (Supporting Information Figure S4). The α value for TF-PIP$_2$ motion at mobile fraction of bilayers carrying QPVP dropped to 0.9, which suggests the diffusive motion of TF-PIP$_2$ switched from Brownian to anomalous motion upon adsorption of QPVP (Supporting Information Figure S4). In principle, confocal FCS can resolve two populations if their diffusion coefficients differ by a factor of ~1.6.[36] If the diffusion coefficients are similar, or if there is a range of mobilities, the anomalous diffusion model will be a better description of the data. For the data presented here, the FCS curves fit better to an anomalous diffusion function than for a function with two time components. The observed decrease in α for the lipid upon QPVP binding shows that polymer adsorption creates a distribution of lipid mobility that on average is slower than free lipid diffusion without the polymer.

Adsorption of QPVP on DOPC SLBs Doped with TopFluor-Phosphatidylserine (TF-PS). In order to have a better understanding of the role electrostatic interactions play in the coupling of anionic lipids and QPVP, DOPC SLBs doped with TF-PS were used. TF-PS has one negative charged phosphate on the headgroup, while TF-PIP$_2$ has three in net. Consequently, TF-PS has lower charge density on the headgroup, which should lead to weaker electrostatic interactions with QPVP compared to TF-PIP$_2$. Upon adsorption of QPVP, two populations of QPVP, immobile and mobile, can be observed in the epi-fluorescence image (Figure 5A). However, no clustering of TF-PS was found, even

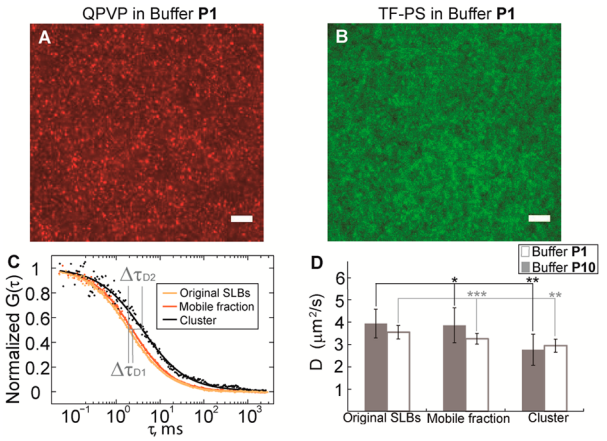

Figure 5. Epi-fluorescence image of TF-PS SLBs carrying QPVP, (A) image of QPVP, (B) image of TF-PS. Scale bars are 5 μm. (C) Autocorrelation curves of TF-PS (buffer **P1**) in original SLBs (orange), at mobile fraction of SLBs carrying QPVP (red) and around cluster of SLBs carrying QPVP (black). (D) The diffusion coefficients of TF-PS in buffer **P10** (gray) and buffer **P1** (white) are shown for each region. The diffusion coefficients are the average of 20 measurements on four SLBs (* p = 0.17, ** p < 0.002, *** p = 0.02).

in the low ionic strength buffer (buffer **P1**, Figure 5B), indicating that the interaction of immobile QPVP is weaker with TF-PS than it is with TF-PIP$_2$.

To understand the behavior of TF-PS interacting with both QPVP populations, the laser excitation beam was positioned in regions corresponding to mobile QPVP and in regions with immobile QPVP clusters. From the autocorrelation curves of TF-PS in regions with immobile QPVP clusters compared to the original bilayer in buffer **P1** (Figure 5C), the lipid mobility changes significantly. The diffusion coefficients of TF-PS with adsorbed QPVP in buffer **P1** (Figure 5D) are 3.26 ± 0.24 $\mu m^2/s$ at mobile fraction and 2.95 ± 0.29 $\mu m^2/s$ around clusters, compared with the diffusion coefficient of TF-PS in the original bilayers, 3.54 ± 0.30 $\mu m^2/s$. Thus, the diffusion coefficient of TF-PS interacting with mobile QPVP is ~16% higher than the diffusion coefficient of TF-PS interacting with immobile QPVP in buffer **P1**.

At higher ionic strength (buffer **P10**), the lipid mobility measured by FCS for bilayer regions with mobile adsorbed QPVP compared to lipids in the original bilayer shows no statistically significant change (p = 0.17) (Figure 5D). This indicates very weak interactions between the lipid and mobile polymer, which remain essentially unchanged over the range of ionic strengths tested. However, around immobile QPVP clusters (Figure 5D) the TF-PS diffusion coefficient is 2.76 ± 0.69 $\mu m^2/s$, which is ~30% lower than in the original bilayers (3.93 ± 0.64 $\mu m^2/s$).

Compared with TF-PIP$_2$ experiments, the slaving effect of TF-PS is less significant, indicating that the interaction between anionic lipids and QPVP is modulated through lipid headgroup charge. Higher headgroup charge resulted in stronger slaving of the lipids, which is further evidence that the coupling between anionic lipid molecules and QPVP is driven by electrostatic interactions. In fact, for buffer **P10**, the diffusion of TF-PS is not affected by QPVP, indicating that the electrostatic interaction is negligible between TF-PS molecules and QPVP

DOI: 10.1021/la504241w
Langmuir 2015, 31, 1784–1791

under biological buffer conditions. As with TF-PIP_2 experiments, we also see no cross-correlation amplitude between QPVP and TF-PS under different buffer conditions as shown in Supporting Information Figure S6.

CONCLUSION

In this study we investigated the diffusion of SLBs containing TF-PIP_2 and TF-PS in response to QPVP adsorption in different buffer conditions. We found the mobility of TF-PIP_2 decreased significantly upon adsorption of QPVP. By tuning the salt concentration of the supporting buffer, we found that the electrostatic interactions between QPVP and TF-PIP_2 could be screened, resulting in a less significant TF-PIP_2 mobility decrease. Overall, the decrease of mobility is evidence that the diffusive motion of lipids and adsorbed polyelectrolytes are coupled, or slaved as indicated in previous reports.[18] Since the strength of interaction between lipids with unmodified headgroups and the cationic polymer is dependent on the ionic strength of supporting buffer, we can conclude that the mobility decrease of TF-PIP_2 due to adsorption of QPVP is driven by electrostatic interactions.

In addition to the correlation between anionic lipid mobility and the ionic strength of the supporting buffer, we also observe a difference in the mobility of TF-PS and TF-PIP_2 in the same buffer. For example, in buffer **P1**, TF-PS mobility upon adsorption of QPVP decreased 8.2%, while the mobility decrease for TF-PIP_2 is 56.6%. This is direct evidence that QPVP has stronger electrostatic interactions with the −3 charged PIP_2 headgroup than with the −1 charged PS headgroup. The dependence of mobility on the headgroup charge density is consistent with conclusions of previous simulation and experimental studies showing that monovalent anionic lipid cannot be sequestered by cationic polyelectrolytes.[5,19,37]

Upon adsorption to lipid bilayers, QPVP was found to divide into two populations. One population is monomeric and highly mobile, and the other population is assembled into immobile polymer aggregates. We observed that the motion of anionic lipids separated into two modes depending on their location on the bilayer compared to QPVP. The mobility of anionic lipids in areas of mobile QPVP is higher than that of lipids in areas corresponding to immobile QPVP clusters. This bifurcation of lipid mobility is analogous to an earlier report by Zhang et al., who observed that the mobility of a headgroup labeled lipid analog in a supported lipid bilayer with adsorbed polymer varied spatially in a bimodal way.[18] In that study, the polymer was not labeled, but was shown to have a high fractional coverage (>20%) compared to the current report (~0.01%). The slow lipid motion was argued to be the collective diffusion of a lipid−macromolecule unit in which lipids were trapped by diffusive polymer nanodomains. In our system, we observe that the lipid mobility of a singly charged anionic lipid (TF-PS) is not significantly slaved to mobile polymer, but is only slowed in the neighborhood of immobile polymer clusters. In addition, our dual-color cross-correlation experiments did not show evidence of correlated lipid/QPVP diffusion, even at low ionic strengths (Supporting Information Figure S5). This suggests that the polyelectrolyte−lipid electrostatic interaction at a low surface coverage is nonspecific, highly dynamic, and unable to form a stable lipid−macromolecule complex.

Together, these measurements show how adsorbed macromolecules alter the mobility of lipid molecules with counter charges according to different electrostatic interaction strengths. Our results demonstrate that the driving force of anionic lipid molecule mobility alteration is electrostatic interaction between the two populations. For freely diffusing polymers, electrostatic interactions are unable to cause any lipid lateral redistribution (e.g., forming macromolecule−lipid nanodomains), and do not significantly alter monovalent lipid mobility under biological buffer conditions. This work offers a new understanding of how anionic lipids are affected by electrostatic interaction with peripheral macromolecules, and will guide future experimental and simulation efforts to decode the dynamics of the lipid−protein interface.

ASSOCIATED CONTENT

Supporting Information

Additional figures with characterization data. This material is available free of charge via the Internet at http://pubs.acs.org.

AUTHOR INFORMATION

Corresponding Author

*E-mail: asmith5@uakron.edu.

Notes

The authors declare no competing financial interest.

ACKNOWLEDGMENTS

The authors would like to thank the University of Akron Research Foundation for supporting this work.

REFERENCES

(1) Lemmon, M. A. Membrane recognition by phospholipid-binding domains. *Nat. Rev. Mol. Cell Biol.* **2008**, *9* (2), 99−111.

(2) Wang, J.; Gambhir, A.; Hangyás-Mihályné, G.; Murray, D.; Golebiewska, U.; McLaughlin, S. Lateral sequestration of phosphatidylinositol 4,5-bisphosphate by the basic effector domain of myristoylated alanine-rich C kinase substrate is due to nonspecific electrostatic interactions. *J. Biol. Chem.* **2002**, *277* (37), 34401−34412.

(3) McLaughlin, S.; Murray, D. Plasma membrane phosphoinositide organization by protein electrostatics. *Nature* **2005**, *438* (7068), 605−611.

(4) Yamazaki, V.; Sirenko, O.; Schafer, R. J.; Groves, J. T. Lipid mobility and molecular binding in fluid lipid membranes. *J. Am. Chem. Soc.* **2005**, *127* (9), 2826−2827.

(5) Golebiewska, U.; Gambhir, A.; Hangyás-Mihályné, G.; Zaitseva, I.; Rädler, J.; McLaughlin, S. Membrane-bound basic peptides sequester multivalent (PIP2), but not monovalent (PS), acidic lipids. *Biophys. J.* **2006**, *91* (2), 588−599.

(6) Gambhir, A.; Hangyás-Mihályné, G.; Zaitseva, I.; Cafiso, D. S.; Wang, J.; Murray, D.; Pentyala, S. N.; Smith, S. O.; McLaughlin, S. Electrostatic sequestration of PIP2 on phospholipid membranes by basic/aromatic regions of proteins. *Biophys. J.* **2004**, *86* (4), 2188−2207.

(7) Vance, J. E.; Steenbergen, R. Metabolism and functions of phosphatidylserine. *Prog. Lipid Res.* **2005**, *44* (4), 207−234.

(8) Di Paolo, G.; De Camilli, P. Phosphoinositides in cell regulation and membrane dynamics. *Nature* **2006**, *443* (7112), 651−657.

(9) Kooijman, E. E.; King, K. E.; Gangoda, M.; Gericke, A. Ionization properties of phosphatidylinositol polyphosphates in mixed model membranes. *Biochemistry* **2009**, *48* (40), 9360−9371.

(10) Czech, M. P. PIP2 and PIP3: Complex roles at the cell surface. *Cell* **2000**, *100* (6), 603−606.

(11) Golebiewska, U.; Nyako, M.; Woturski, W.; Zaitseva, I.; McLaughlin, S. Diffusion coefficient of fluorescent phosphatidylinositol 4,5-bisphosphate in the plasma membrane of cells. *Mol. Biol. Cell* **2008**, *19* (4), 1663−1669.

(12) Duan, X.; Zhang, R.; Li, Y.; Shi, T.; An, L.; Huang, Q. Monte Carlo Study of polyelectrolyte adsorption on mixed lipid membrane. *J. Phys. Chem. B* **2013**, *117* (4), 989−1002.

DOI: 10.1021/la504241w
Langmuir 2015, 31, 1784−1791

(13) Khelashvili, G.; Weinstein, H.; Harries, D. Protein diffusion on charged membranes: A dynamic mean-field model describes time evolution and lipid reorganization. *Biophys. J.* **2008**, *94* (7), 2580−2597.
(14) Mbamala, E. C.; Ben-Shaul, A.; May, S. Domain formation induced by the adsorption of charged proteins on mixed lipid membranes. *Biophys. J.* **2005**, *88* (3), 1702−1714.
(15) Rusu, L.; Gambhir, A.; McLaughlin, S.; Rädler, J. Fluorescence correlation spectroscopy studies of peptide and protein binding to phospholipid vesicles. *Biophys. J.* **2004**, *87* (2), 1044−1053.
(16) van den Bogaart, G.; Meyenberg, K.; Risselada, H. J.; Amin, H.; Willig, K. I.; Hubrich, B. E.; Dier, M.; Hell, S. W.; Grubmuller, H.; Diederichsen, U.; Jahn, R. Membrane protein sequestering by ionic protein-lipid interactions. *Nature* **2011**, *479* (7374), 552−555.
(17) Yeung, T.; Gilbert, G. E.; Shi, J.; Silvius, J.; Kapus, A.; Grinstein, S. Membrane phosphatidylserine regulates surface charge and protein localization. *Science* **2008**, *319* (5860), 210−213.
(18) Zhang, L.; Granick, S. Slaved diffusion in phospholipid bilayers. *Proc. Natl. Acad. Sci. U.S.A.* **2005**, *102* (26), 9118−9121.
(19) Kiselev, V. Y.; Marenduzzo, D.; Goryachev, A. B. Lateral dynamics of proteins with polybasic domain on anionic membranes: A dynamic Monte-Carlo study. *Biophys. J.* **2011**, *100* (5), 1261−1270.
(20) Tzlil, S.; Ben-Shaul, A. Flexible charged macromolecules on mixed fluid lipid membranes: Theory and Monte Carlo simulations. *Biophys. J.* **2005**, *89* (5), 2972−2987.
(21) Tzlil, S.; Murray, D.; Ben-Shaul, A. The "electrostatic-switch" mechanism: Monte Carlo study of MARCKS-membrane interaction. *Biophys. J.* **2008**, *95* (4), 1745−1757.
(22) Comar, W. D.; Schubert, S. M.; Jastrzebska, B.; Palczewski, K.; Smith, A. W. Time-resolved fluorescence spectroscopy measures clustering and mobility of a G protein-coupled receptor opsin in live cell membranes. *J. Am. Chem. Soc.* **2014**, *136* (23), 8342−8349.
(23) Endres, N. F.; Das, R.; Smith, A. W.; Arkhipov, A.; Kovacs, E.; Huang, Y.; Pelton, J. G.; Shan, Y.; Shaw, D. E.; Wemmer, D. E.; Groves, J. T.; Kuriyan, J. Conformational coupling across the plasma membrane in activation of the EGF receptor. *Cell* **2013**, *152* (3), 543−556.
(24) Lai, J. T.; Filla, D.; Shea, R. Functional polymers from novel carboxyl-terminated trithiocarbonates as highly efficient RAFT agents. *Macromolecules* **2002**, *35* (18), 6754−6756.
(25) Bacia, K.; Schwille, P. Practical guidelines for dual-color fluorescence cross-correlation spectroscopy. *Nat. Protoc.* **2007**, *2* (11), 2842−2856.
(26) Müller, B. K.; Zaychikov, E.; Bräuchle, C.; Lamb, D. C. Pulsed interleaved excitation. *Biophys. J.* **2005**, *89* (5), 3508−3522.
(27) Coyle, M. P.; Xu, Q.; Chiang, S.; Francis, M. B.; Groves, J. T. DNA-mediated assembly of protein heterodimers on membrane surfaces. *J. Am. Chem. Soc.* **2013**, *135* (13), 5012−5016.
(28) Reiner, A.; Ledjeff, K. Anion exchange membranes consisting of poly (vinylpyridine) and poly (vinylbenzyl chloride) for cr/fe redox batteries. *J. Membr. Sci.* **1988**, *36* (0), 535−540.
(29) Chetouani, A.; Medjahed, K.; Al-Deyab, S. S.; Hammouti, B.; Warad, I.; Mansri, A.; Aouniti, A. Inhibition of corrosion of pure iron by quaternized poly(4-vinylpyridine)-graft-bromodecane in sulphuric acid. *Int. J. Electrochem. Sci.* **2012**, *7* (7), 6025−6043.
(30) Sellenet, P. H.; Allison, B.; Applegate, B. M.; Youngblood, J. P. Synergistic activity of hydrophilic modification in antibiotic polymers. *Biomacromolecules* **2006**, *8* (1), 19−23.
(31) San Juan, A.; Letourneur, D.; Izumrudov, V. A. Quaternized poly(4-vinylpyridine)s as model gene delivery polycations: Structure−function study by modification of side chain hydrophobicity and degree of alkylation. *Bioconjugate Chem.* **2007**, *18* (3), 922−928.
(32) Keddie, D. J. A guide to the synthesis of block copolymers using reversible-addition fragmentation chain transfer (RAFT) polymerization. *Chem. Soc. Rev.* **2014**, *43* (2), 496−505.
(33) Braunger, J. A.; Kramer, C.; Morick, D.; Steinem, C. Solid supported membranes doped with PIP2: Influence of ionic strength and ph on bilayer formation and membrane organization. *Langmuir* **2013**, *29* (46), 14204−14213.
(34) Yanez Arteta, M.; Ainalem, M.-L.; Porcar, L.; Martel, A.; Coker, H.; Lundberg, D.; Chang, D. P.-S.; Soltwedel, O.; Barker, R. D.; Nylander, T. Interactions of PAMAM dendrimers with negatively charged model biomembranes. *J. Phys. Chem. B* **2014**, *118*, 12892−12906.
(35) Zimmermann, R.; Küttner, D.; Renner, L.; Kaufmann, M.; Zitzmann, J.; Müller, M.; Werner, C. Charging and structure of zwitterionic supported bilayer lipid membranes studied by streaming current measurements, fluorescence microscopy, and attenuated total reflection Fourier transform infrared spectroscopy. *Biointerphases* **2009**, *4* (1), 1−6.
(36) Meseth, U.; Wohland, T.; Rigler, R.; Vogel, H. Resolution of fluorescence correlation measurements. *Biophys. J.* **1999**, *76* (3), 1619−1631.
(37) Duan, X.; Li, Y.; Zhang, R.; Shi, T.; An, L.; Huang, Q. Regulation of anionic lipids in binary membrane upon the adsorption of polyelectrolyte: A Monte Carlo simulation. *AIP Adv.* **2013**, *3* (6), 062128.

DOI: 10.1021/la504241w
Langmuir 2015, 31, 1784−1791